ISSN 2663-1563 Vol. 8, Issue 1: 28-36, DOI: 10.25236/AJAGE.2026.080104

Tensile Behaviors and Interfacial Slip of Hydraulic Lime-modified Earthen Matrix Composites Reinforced with Glass Fiber Mesh

Long Zhou[1,a], Xuming Zhang[1], Haotian Guo[1], Feng Wu[1,b,*]

[1]School of Transportation Engineering, Dalian Jiaotong University, Dalian, 116028, China
[a]2209048450@qq.com, [b]wfdjtu@sina.com
[*]Corresponding author

Abstract: *Interfacial slip between the glass fiber mesh and the modified earthen matrix remains a critical issue in fiber-reinforced earthen matrix (FREM) retrofitting,as it significantly impairs the load-bearing capacity of traditional earthen structures. To address this issue, a three-dimensional finite element model was developed to simulate the nonlinear contact behavior between the fiber mesh and the modified matrix. The framework incorporates a damaged plasticity model for the earthen matrix and employs a global surface-to-surface contact algorithm to capture progressive interfacial slip and debonding. The reliability of the numerical model was validated against direct tensile test results, yielding a prediction error of less than 8% for the ultimate tensile strength. Subsequently, comprehensive parametric analyses were conducted to evaluate the effects of matrix modifier types, clamping configurations, and anchorage lengths. Results indicate that the artificial hydraulic lime (AHL) modified system exhibited a 30.1% higher ultimate tensile strength compared to the natural hydraulic lime (NHL) counterpart. Furthermore, an anchorage length of 100 mm triggered sudden slip failure, whereas extending the length to 150 mm transitioned the failure mode to progressive debonding, enhancing the tensile strength by 20%. However, further extension to 200 mm yielded only a marginal 3% strength gain, indicating an optimal anchorage threshold. Damage evolution analysis revealed an asymmetric failure mechanism dominated by end damage, highlighting that plastic damage and shear stress are consistently concentrate at the anchorage ends. These findings provide a robust quantitative basis for the parameter optimization and standardized testing of FREM reinforcement systems.*

Keywords: *Earthen matrix; Numerical modelling; Composites; Tensile behavior; Interfacial slip*

1. Introduction

Recently, fiber-reinforced earthen matrix (FREM) composites have emerged as a sustainable and mechanically efficient retrofitting solution for traditional earthen structures[1-6]. However, the inherently weak interfacial bonding between the earthen matrix and the glass fiber mesh inevitably leads to premature interfacial slip under uniaxial tension. This phenomenon severely hinders stress transfer, preventing the fiber mesh from exerting its full reinforcing potential and ultimately compromising the load-bearing capacity of the FREM system [7].

Strengthening the physical and mechanical characteristics of the matrix material serves as a practical method for reducing interfacial slip[8]. While previous studies have explored matrix modifications with waterborne polyurethanes or chopped fibers, these empirical approaches fail to fundamentally address the issue of insufficient interfacial adhesion[9-11]. As a novel inorganic modifier, hydraulic lime (HL) has recently attracted significant attention. Unlike conventional air-hardening lime, the dense C-S-H gel network generated during HL hydration markedly enhances the micro-density and mechanical strength of the matrix [12-14]. Nevertheless, existing literature on HL-modified composites is overwhelmingly limited to cementitious or mortar matrices, and its synergistic application with continuous fiber meshes in earthen structures has not been systematically investigated[15-17].

Furthermore, current evaluations of FREM load-transfer mechanisms rely predominantly on macroscopic tensile tests[9,18]. These empirical methods are fundamentally limited in capturing the dynamic internal multi-crack evolution, microscopic stress transfer pathways, and progressive interfacial slip phenomena. To bridge this gap, numerical modeling offers a robust analytical alternative. While the Concrete Damaged Plasticity (CDP) model has proven effective in characterizing the nonlinear behavior

ISSN 2663-1563 Vol. 8, Issue 1: 28-36, DOI: 10.25236/AJAGE.2026.080104

of earthen materials[19], and various refined models exist for standard FRCM composites, a comprehensive 3D numerical framework explicitly accounting for the complex nonlinear interfacial slip within HL-modified FREM systems is notably absent.

To address these distinct material and methodological limitations, this study develops a refined three-dimensional finite element (FE) model to investigate the dynamic tensile response and interfacial slip mechanisms of glass fiber mesh-reinforced HL-modified earthen composites. Incorporating a global surface-to-surface contact algorithm and the CDP constitutive law, the model's reliability was rigorously validated against experimental stress-strain responses and failure modes. Subsequently, extensive parametric analyses were executed to quantify the coupled effects of HL modification types, gripping constraints, and effective anchorage lengths. Ultimately, by elucidating the equivalent plastic damage evolution and interfacial stress distribution, this research provides a vital numerical foundation for the optimization and standardized testing of next-generation FREM retrofitting technologies.

2. Finite Element Modeling

2.1 Geometry and Material Constitutive Models

A 3D meso-scale finite element (FE) model was developed to simulate the uniaxial tensile response and interfacial debonding mechanisms of the FREM composites. The modeled geometry was designed to precisely replicate the experimental specimens[18], which consists of three distinct components: the modified earthen matrix, the glass fiber mesh (thickness: 0.1 mm), and the steel loading fixtures. To investigate the dimensional effects and required anchorage length, the matrix length was parameterized as 500, 600, and 700 mm, with a constant cross-section of 40 mm × 10 mm.

Given the phenomenological similarities between modified earthen matrices and plain concrete [20,21], the Concrete Damaged Plasticity (CDP) model was adopted to govern the inelastic behavior and progressive damage evolution of the earthen matrix[22]. The elastic and strength parameters for both AHL- and NHL-modified matrices were calibrated based on existing experimental data [18]. Specifically, the AHL-modified matrix has an elastic modulus of 102.4 MPa, a tensile strength of 0.192 MPa, and a peak strain of 0.0141. Conversely, the NHL-modified counterpart possesses values of 79.9 MPa, 0.145 MPa, and 0.0103, respectively. A constant Poisson's ratio of 0.3 was assigned to both matrices.

2.2 Interfacial Contact Formulations

The fidelity of the numerical model heavily relies on the precise definition of interfacial behaviors. Perfect displacement continuity between the loading fixtures and the matrix was achieved by applying tie constraints. During the initial model calibration phase, tie constraints were also temporarily applied between the fiber mesh and the matrix within the gripping regions to stabilize the boundary conditions. However, to accurately capture the actual progressive debonding and slip failure mechanisms, the optimized finite element model replaced these local tie constraints with a global surface-to-surface contact algorithm applied to the entire interfacial domain. The overall contact and interaction definitions implemented in the FE model are comprehensively illustrated in Figure 1.

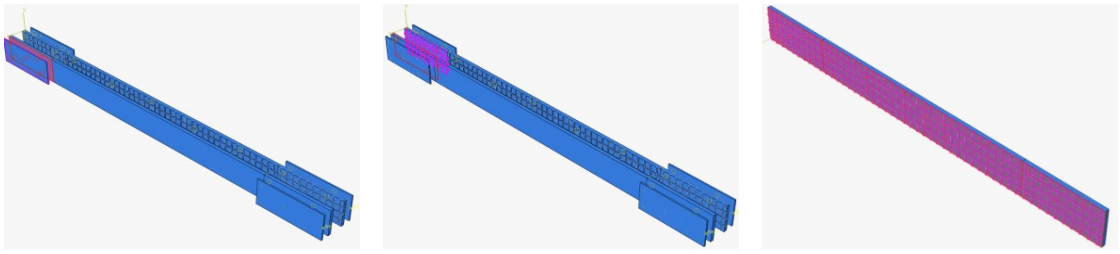

(a) *(b)* *(c)*

Figure 1: Contact and interaction definitions in the FE model: (a) Tie constraints between the loading fixtures and the modified earthen matrix; (b) Initial tie constraints between the matrix and glass fiber mesh at the gripping ends (subsequently relaxed); (c) Global surface-to-surface contact simulating progressive interfacial debonding in the unbonded region.

This global contact formulation adopted a node-to-surface discretization method with a small-sliding tracking approach. The interfacial cohesive behavior was governed by a bilinear traction-separation law calibrated from literature[23]. For the AHL-modified interface, the peak shear stress was 0.442 MPa

ISSN 2663-1563 Vol. 8, Issue 1: 28-36, DOI: 10.25236/AJAGE.2026.080104

corresponding to a relative slip of 0.46 mm. This was followed by a constant residual frictional stress of 0.033 MPa at a total ultimate slip of 1.533 mm. Similarly, the NHL-modified interface exhibited a peak shear stress of 0.336 MPa corresponding to a relative slip of 0.63 mm, followed by a residual frictional stress of 0.002 MPa at a total ultimate slip of 1.533 mm.

2.3 Boundary Conditions and Loading Protocols

To effect the influence of boundary confinement on failure mechanisms, two standardized gripping configurations—clevis grips (U-type) and clamping grips (C-type)[24]—were incorporated into the model, as shown in Figure 2. A uniform gripping length of 100 mm was maintained across all configurations. One end of the specimen was fully restrained against translation, while a monotonically increasing axial displacement was applied to the opposite end to replicate quasi-static tensile loading conditions. For models adopting the C-type clamping configuration, an additional out-of-plane (normal) compressive pressure was uniformly applied to the fixture surfaces to simulate the transverse confinement caused by bolt fastening.

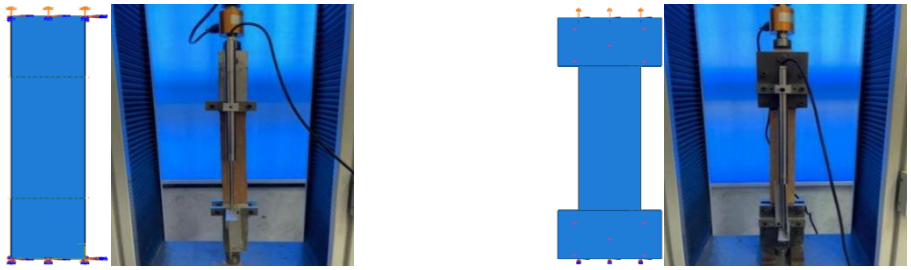

(a)U-type clevis grip setup *(b)C-type clamping grip setup*

Figure 2: Standardized gripping configurations and boundary conditions.

2.4 Element Selection and Mesh Discretization

All spatial domains (matrix, fiber mesh, and fixtures) were discretized using 8-node linear brick elements with reduced integration and hourglass control (C3D8R). This element type effectively suppresses zero-energy modes while ensuring computational efficiency during the stable tracking of post-cracking plastic damage evolution. Based on preliminary mesh sensitivity analyses[25], a global characteristic element size of 5 mm was assigned to the earthen matrix and fixtures. To accurately capture the localized high-stress gradients and progressive debonding at the interface, the mesh density within the glass fiber mesh region was locally refined to 1 mm, as depicted in Figure 3. This mesh discretization strategy achieves an optimal balance between numerical convergence and computational efficiency.

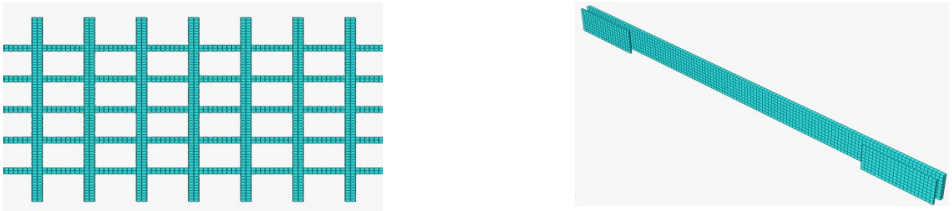

(a)Localized mesh refinement for the glass fiber mesh *(b)Global mesh allocation for the modified earthen matrix and steel fixtures*

Figure 3: Mesh discretization strategy.

2.5 Parametric Simulation Matrix

To systematically investigate the combined effects of geometric and material parameters on the tensile response of FREM composites, a comprehensive parametric simulation matrix was established. As detailed in Table 1, this matrix encompasses baseline validation, matrix size effects, and anchorage characteristics evaluation.

ISSN 2663-1563 Vol. 8, Issue 1: 28-36, DOI: 10.25236/AJAGE.2026.080104

Table 1 Parametric simulation matrix for the FREM composite configurations.

Specimen ID	Matrix Modifier	Matrix length mm	Gripping length mm	Gripping Configuration	Z-direction constraint
NHLE-500-100	NHL	500	100	U-type	No
AHLE-500-100	AHL	500	100	U-type	No
AHLJ-500-100	AHL	500	100	U-type	No
AHLJ-600-100	AHL	600	100	U-type	No
AHLJ-700-100	AHL	700	100	U-type	No
AHLJZ-500-100	AHL	500	100	C-type	Yes
AHLJZ-600-100	AHL	600	100	C-type	Yes
AHLJZ-700-100	AHL	700	100	C-type	Yes
AHL-500-100	AHL	500	100	U-type	No
AHL-600-150	AHL	600	150	U-type	No
AHL-700-200	AHL	700	200	U-type	No
NHL-500-100	NHL	500	100	U-type	No
NHL-600-150	NHL	600	150	U-type	No
NHL-700-200	NHL	700	200	U-type	No
AHLZ-500-100	AHL	500	100	C-type	Yes
AHLZ-600-150	AHL	600	150	C-type	Yes
AHLZ-700-200	AHL	700	200	C-type	Yes
NHLZ-500-100	NHL	500	100	C-type	Yes
NHLZ-600-150	NHL	600	150	C-type	Yes
NHLZ-700-200	NHL	700	200	C-type	Yes

(Note: NHLE = Natural hydraulic lime-modified earthen specimen; AHLJ = Artificial hydraulic lime-modified specimen with parameterized anchorage length; AHLZ = Artificial hydraulic lime-modified specimen with C-type clamp configuration.)

3. Results and Discussion

3.1 Benchmark Finite Element Model Validation

To validate the reliability of the proposed global contact finite element framework, the simulated uniaxial tensile stress-strain curves and damage evolution characteristics were extracted and compared with representative experimental data of FREM composites[26]. As illustrated in Figure 4, the numerical model accurately reproduces the mechanical response of the specimens across both the elastic and strain-hardening phases. During the linear elastic stage, the stress-strain gradients of the simulated and experimental curves virtually coincide. For instance, the stiffness deviation of the NHLE-500-100 specimen is only 4.5%, which indicates that the model effectively captures the initial synergistic load-bearing mechanism between the matrix and the glass fiber mesh. After yielding, the simulation captures the progressive work-hardening behavior through the continuous damage constitutive model, which is in excellent agreement with the experimental results.

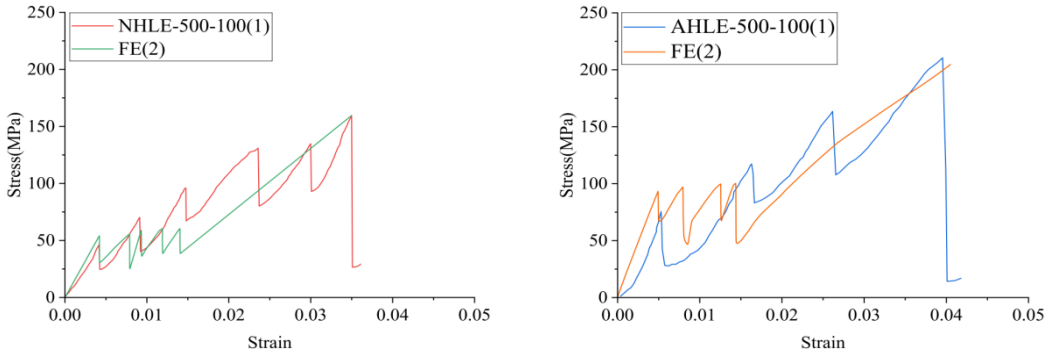

(a) NHLE-500-100 specimen *(b) AHLE-500-100 specimen*

Figure 4: Validation of stress-strain responses against experimental data.

Quantitatively, the relative errors between the numerical predictions and experimental measurements

ISSN 2663-1563 Vol. 8, Issue 1: 28-36, DOI: 10.25236/AJAGE.2026.080104

for both cracking strength and ultimate tensile strength are strictly bounded within 8%. Crucially, the implementation of the global surface-to-surface contact algorithm enables the model to successfully capture the interfacial slip and subsequent debonding failure stage of the fiber mesh, which was explicitly observed during the physical tests. In contrast, conventional simplified tie constraints inherently suppress end slip, thus failing to reproduce the actual ultimate failure state. Furthermore, comparing the equivalent plastic damage contours，as shown in Figure 5, the model accurately predicts the transverse crack distribution and propagation paths within the FREM structure, further corroborating its validity for complex mechanical mechanism analysis.

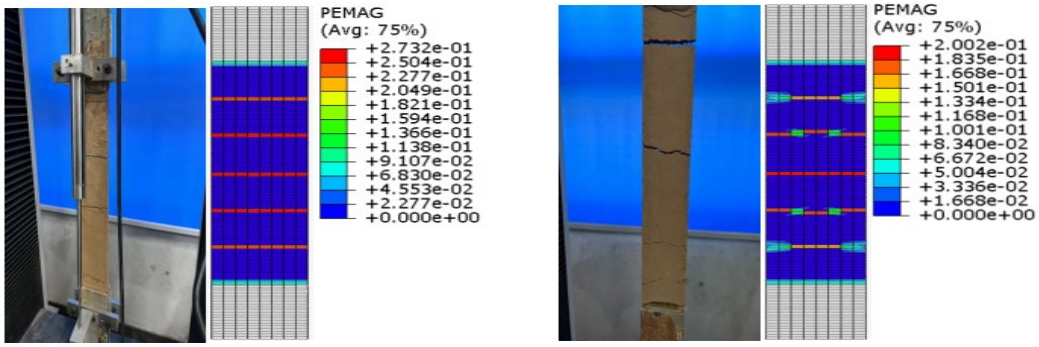

(a) NHLE-500-100 specimen *(b) AHLE-500-100 specimen*

Figure 5: Comparison of failure modes and transverse crack distributions.

3.2 Parametric Analysis and Macroscopic Mechanical Response

Following model validation, a comprehensive parametric study was conducted to evaluate the isolated and coupled effects of matrix modification types, geometric scaling (matrix length), anchorage lengths, and gripping configurations on the tensile performance of the FREM composites.

The type of matrix modifier fundamentally determines the ultimate strength of the system. For specimens with identical dimensions, the ultimate tensile strength of the artificial hydraulic lime (AHL) modified system is 30.1% higher than that of the natural hydraulic lime (NHL) counterpart. This significant improvement is attributed to the denser C-S-H gel network formed during AHL hydration, which greatly enhances the microstructural integrity and mechanical interlocking at the interfacial transition zone, thus reducing stress dissipation caused by premature interfacial slip.

Regarding the dimensional effect, the analysis of different matrix lengths in Figure 6 shows that under the short anchorage condition of 100 mm, simply extending the overall matrix length does not change the fundamental failure mechanism of sudden interfacial slip.Across both gripping configurations, the stress-strain curves exhibit an identical failure pattern characterized by an abrupt post-peak stress drop, with negligible variations in the peak tensile strength. However, as the matrix length increases from 500 mm to 700 mm, the peak strain corresponding to the ultimate stress decreases significantly. This phenomenon indicates that a longer matrix results in a more uniform stress distribution under tensile loading, thus reducing the rate of localized strain accumulation.

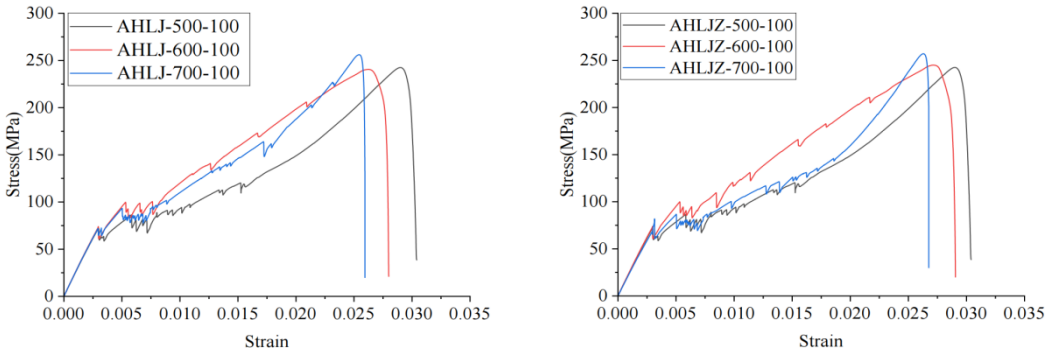

(a) U-type configuration (AHLJ series) *(b) C-type configuration (AHLJZ series)*

Figure 6: Influence of matrix length on the stress-strain responses of AHL-modified earthen composites.

ISSN 2663-1563 Vol. 8, Issue 1: 28-36, DOI: 10.25236/AJAGE.2026.080104

Anchorage length emerges as the governing parameter dictating the interfacial failure mode, as elucidated in Figure 7 and Figure 8. At an insufficient anchorage length of 100 mm, the effective interfacial contact area is inadequate. When the interfacial shear stress reaches the cohesive strength, sudden global slip failure occurs, leading to a sharp drop in load-bearing capacity. Extending the anchorage length to 150 mm transitions the failure mechanism to progressive debonding, yielding a substantial 20% increase in ultimate tensile strength compared to the 100 mm baseline. Nevertheless, further extension to 200 mm provides a marginal strength gain of merely 3%, evidencing a pronounced diminishing marginal utility in strength enhancement. This indicates that 150 mm serves as the critical optimal anchorage length, balancing material efficiency with mechanical capacity.

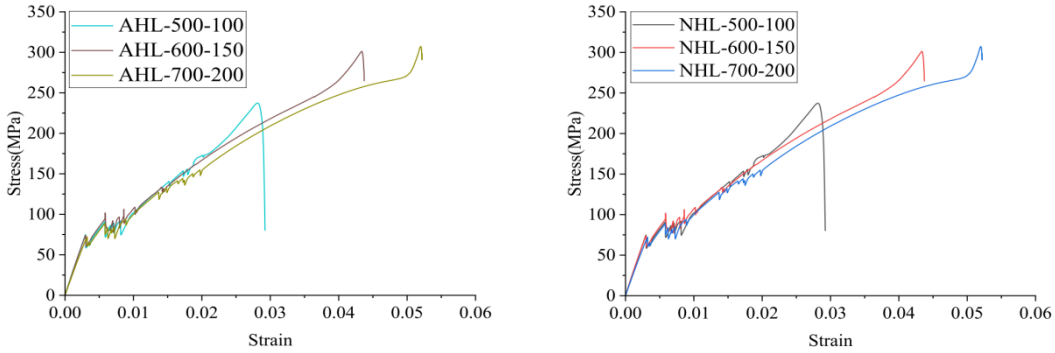

(a)AHL-modified specimens *(b)NHL-modified specimens*

Figure 7: Effect of anchorage length on the stress-strain behavior under U-type clevis grips.

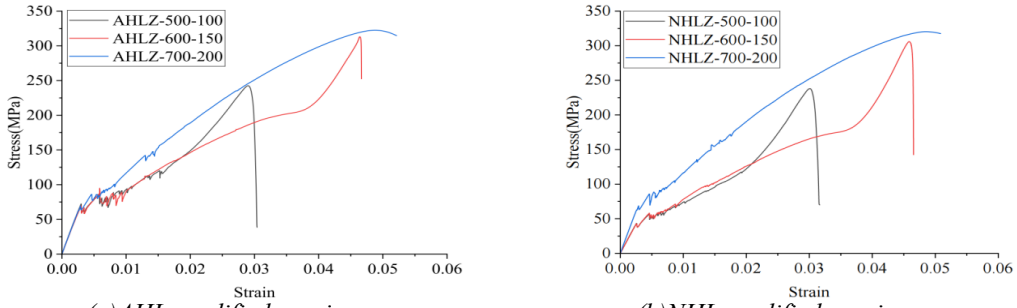

(a)AHL-modified specimens *(b)NHL-modified specimens.*

Figure 8: Effect of anchorage length on the stress-strain behavior under C-type clamping grips.

Furthermore, the gripping configuration profoundly influences the post-peak load redistribution pathways. Under U-type clevis constraints, the specimens show a sudden increase in stiffness near the peak load. This phenomenon occurs because when the matrix cracks fully propagate and the matrix loses its load-bearing capacity, the tensile force is immediately transferred to the unbonded glass fiber mesh. In contrast, the C-type clamping grip, providing robust out-of-plane normal confinement, ensures a smoother load transfer without severe stress mutations. Its mechanical response more accurately reflects the synergistic stress patterns observed in authentic engineering retrofitting overlays.

3.3 Failure Mechanism and Interfacial Stress Transfer Law

To elucidate the micromechanical mechanisms driving these macroscopic responses, stress distributions within the glass fiber mesh and equivalent plastic damage contours of the matrix were extracted across varying anchorage lengths

The analysis of stress transfer efficiency indicates that the overall stress distribution patterns in the fiber mesh are phenomenologically consistent across different gripping configurations and matrix modification systems. The fundamental disparities in mechanical responses across varying anchorage lengths stem directly from how the bonded length regulates interfacial adhesion and shear stress allocation. As depicted in Figure 9, under the inadequate 100 mm anchorage condition, the high-stress region within the fiber mesh is severely localized at the specimen's mid-span, leaving the extensive flanking areas at near-zero stress levels. This indicates that shear stresses are excessively concentrated at the anchorage ends, which causes the cohesive strength to be exceeded prematurely before the continuous fiber mesh can exert its full tensile potential. Conversely, when the anchorage length is extended to 150 mm and beyond, the high-stress zone propagates uniformly across the entire fiber domain. This mitigates

ISSN 2663-1563 Vol. 8, Issue 1: 28-36, DOI: 10.25236/AJAGE.2026.080104

detrimental local stress concentrations, shifting the load-transfer paradigm from localized bearing to global synergy, thereby drastically elevating the structural load-carrying capacity.

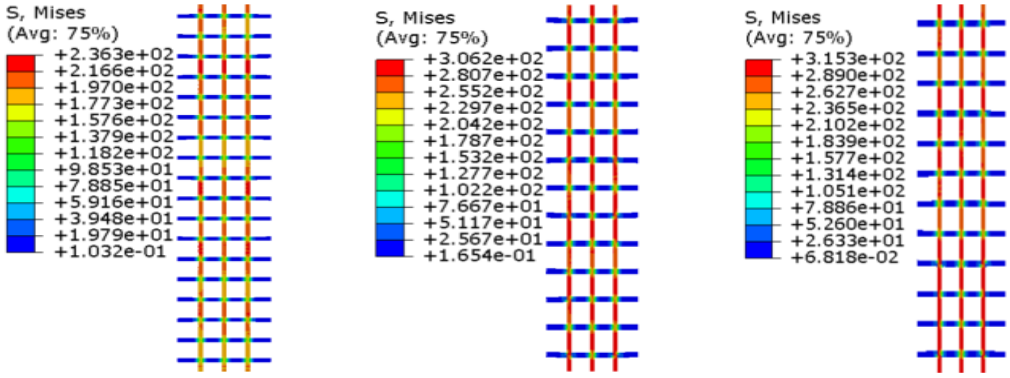

(a)100 mm *(b)150 mm* *(c)200 mm*

Figure 9: Stress distribution contours of the glass fiber mesh under varying anchorage lengths.

As illustrated in Figure 10, the damage evolution profiles further expose an asymmetric end-damage-dominated failure characteristic intrinsic to FREM systems. Throughout the tensile loading history, plastic damage inexorably accumulates toward the anchorage ends. Although extending the anchorage length results in more uniform stress transfer in the central region, thus maintaining a micro-damage state, the clamping ends—acting as the absolute boundaries for load transfer—experience increased shear stress accumulation and more severe peak damage as the effective bonded length increases. This micromechanical insight explains the exacerbated end-damage observed in longer anchorage configurations and establishes a critical theoretical basis for optimizing the anchorage design in standardized direct tensile tests for FREM structures.

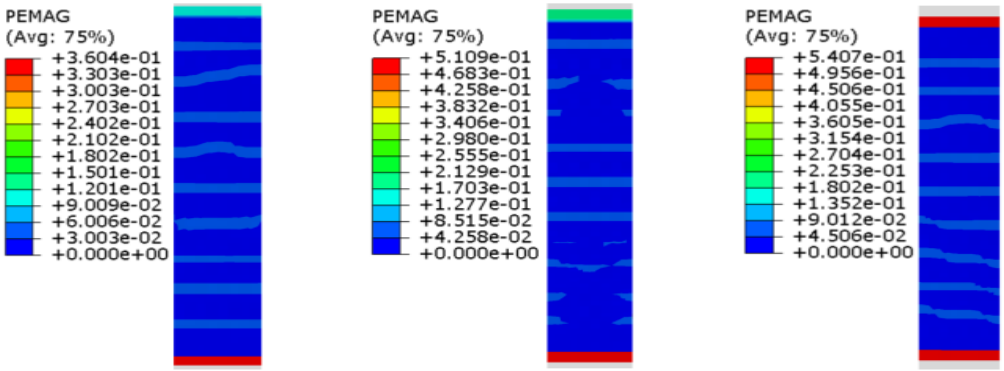

(a) 100 mm *(b)150 mm* *(c)200 mm*

Figure 10: Equivalent plastic damage evolution in the modified earthen matrix under varying anchorage lengths.

4. Conclusions

To address the interfacial slip bottleneck in FREM retrofitting systems under uniaxial tension, a refined three-dimensional finite element model incorporating nonlinear interfacial contact was developed. Based on rigorous experimental validation and comprehensive parametric analyses, the following principal conclusions are drawn:

(1) The numerical framework, which adopts a global surface-to-surface contact algorithm, accurately captures the tensile mechanical behavior of FREM composites and predicts the ultimate tensile strength with a relative error of less than 8%.Overcoming the artificial constraints of conventional tie constraint methods, this contact formulation accurately reproduces the progressive interfacial slip and subsequent debonding failure of the glass fiber mesh.

(2) The type of matrix modifier and the gripping configuration jointly determine the anti-slip performance of the FREM system. The artificial hydraulic lime (AHL) modified system yields a 30.1% higher ultimate load-bearing capacity than its natural counterpart (NHL), as its denser hydration products

ISSN 2663-1563 Vol. 8, Issue 1: 28-36, DOI: 10.25236/AJAGE.2026.080104

significantly enhance interfacial mechanical interlocking. Regarding boundary conditions, the out-of-plane normal confinement provided by C-type clamps mitigates post-cracking stress mutations, ensuring a far more stable load transfer compared to unconfined U-type grips.

(3) Anchorage length is the fundamental determinant of the interfacial failure mechanism and reinforcement efficiency. An insufficient anchorage length of 100 mm leads to insufficient interfacial shear capacity and sudden global slip failure. Extending the anchorage to 150 mm transitions the failure to a progressive mode, optimally enhancing the tensile capacity. However, exceeding this critical threshold yields diminishing marginal returns in strength. This confirms that there exists an optimal anchorage length for practical retrofitting applications, and arbitrarily extending the lap length yields no significant mechanical benefits.

(4) The tensile failure mechanism of the FREM system is heavily dominated by test boundary end-damage. While extending the anchorage interval homogenizes stress distribution in the mid-span, it paradoxically intensifies shear stress concentrations and cumulative damage at the clamping ends. This highlights the "end effect" as a critical variable in tensile performance evaluation. Future development of standardized direct tensile test methods for FREM composites should prioritize the optimization of end anchorage and clamping fixtures to avoid underestimating the actual load-bearing capacity of the composite system due to premature localized failure.

Acknowledgements

The authors are grateful to the supports of the National Natural Science Foundation of China, (Grant No. 51708082).

References

[1] Carozzi F.G., Poggi C. Mechanical properties and debonding strength of Fabric Reinforced Cementitious Matrix (FRCM) systems for masonry strengthening[J].Composites Part B, 2014, 70215-230.

[2] Hamid Saadatmanesh. Fiber Composites for New and Existing Structures. Structural Journal, 1994, 91.3.

[3] Arboleda, D., Loreto, G., De Luca, A., Nanni, A. Material characterization of fiber reinforced cementitious matrix (FRCM) composite laminates. In: Proceedings for 10th international symposium on ferrocement and thin reinforced cement composite, Havana, 2012.

[4] W. Han, F. Wu, Y. Cheng, H. Wang, S. Chu, Compressive performance of adobe masonry strengthened with glass-fiber reinforced matrix composites, Mater. Struct, 2023, 56(3)1-14.

[5] Mezrea PE, Ispir M, Balci IA, Bal IE, Ilki A. Diagonal tensile tests on historical brick masonry wallets strengthened with fabric reinforced cementitious mortar. Structures, 2023, 33:935–46.

[6] Antonio R ,V. D O ,A. R S .Experimental Investigation on the Bond Behavior of a Compatible TRM-based Solution for Rammed Earth Heritage[J].International Journal of Architectural Heritage, 2019, 13(7):1042-1060.

[7] Z. Zhao, D. Qi, L. Wang, et al. Research progress on glass fiber interface modification and mechanical properties of its composites. Journal of Textile Science and Engineering, 2023, 40(3), 120-125, 138.

[8] Daneshvar K ,Moradi J M ,Roshan N , et al. Enhancing flexural and shear capacities of RC T-beams with FRCM incorporating a full FRCM-concrete bond[J].Construction and Building Materials, 2025, 471,140687.

[9] J. Cui. Glass fiber mesh reinforced rammed earth surface layer tensile performance experimental study (Master's thesis, Dalian Jiaotong University), 2022.

[10] J. Zhang, W. Wang, G. Li. Comparative study on compressive strength test of two natural fiber modified rammed earth specimens. Building Technology, 2024, 55(06), 715–718.

[11] Huimei Z ,Xingzi W ,Jiani C , et al. Effectiveness and compatibility of fabricated hydrauliclime prepared with ultrafine pozzolanic materials in consolidating soil-matrix[J]. Constructionand Building Materials, 2023, 378.

[12] Frank T ,Zimmermann I ,Horn R .Lime application in marshlands of Northern Germany—Influence of liming on the physicochemical and hydraulic properties of clayey soils[J].Soil& Tillage Research, 2020, 204.

[13] J. Wang, Y. Zhang, Y. Lv, et al. (2025). Research progress on hydraulic lime for architectural heritage restoration. Materials Review, 2025, 39(22), 69-81.

ISSN 2663-1563 Vol. 8, Issue 1: 28-36, DOI: 10.25236/AJAGE.2026.080104

[14] J. Yang,W. Song, Wang, L. Wang, et al. Study on synthesis of hydraulic lime from Jiangshi and its physical-mechanical properties. Journal of Rock Mechanics and Engineering, 2018, 37(07), 1766-1775.
[15] S. Yin,S. Xu,F. Wang. Bonding and lap performance of fiber woven mesh in fine-grained concrete. Journal of Building Materials, 2012, 15(01), 34-41.
[16] Falchi L ,Varin C ,Toscano G , et al. Statistical analysis of the physical properties and durability of water-repellent mortars made with limestone cement, natural hydraulic lime and pozzolana-lime[J].Construction and Building Materials, 2015, 78260-270.
[17] Lanas J ,Bernal P J ,Bello M , et al. Mechanical properties of natural hydraulic lime-basedmortars[J]. Cement and Concrete Research, 2004, 34(12):2191-2201.
[18] H. Guo. Research on tensile performance of glass fiber mesh reinforced hydraulic lime-modified rammed earth surface layer (Master's thesis, Dalian Jiaotong University), 2023.
[19] X. Shi, Y. Yao, L. Wang, et al. Influence of CDP model parameters based on uniaxial tension and compression simulation. Building Structures, 2021, 51(S2), 999–1007.
[20] F. Cai, Study on mechanical properties of the soil material with chemical reinforcement,(Master's thesis, Dalian Jiaotong University), 2017.
[21] J. Zhong, Study and application on constitutive relationship for earth material and mechanical compressed earth brick masonry, Chang'an University, Xi'an, China, 2018.
[22] G. Mazzucco, T. D'Antino, C. Pellegrino, V. Salomoni, Three-dimensional finite element modeling of inorganic-matrix composite materials using a mesoscale approach, Compos. PartB Eng. 2018,143,75–85.
[23] X. Liang. Study on the bonding performance between hydraulic lime modified raw soil surface layer and raw soil matrix (Master's thesis, Dalian Jiaotong University), 2024.
[24] Hartig J ,Jesse F ,Schicktanz K , et al. Influence of experimental setups on the apparent uniaxial tensile load-bearing capacity of Textile Reinforced Concrete specimens[J].Materials and Structures, 2012, 45(3):433-446.
[25] X. Zhu, M. Su, Y. Wang, T. Ueda, Numerical and theoretical investigation on the constitutive model of graphene-enhanced FRCM composite, J. Build. Eng, 2024,108734.
[26] ASTM D2487-23, Standard practice for classification of soils for engineering purposes (unified soil classification system), ASTM International, West Conshohocken, 2023.